Journal of Organometallic Chemistry 745-746 (2013) 166–172

Contents lists available at ScienceDirect

Journal of Organometallic Chemistry

journal homepage: www.elsevier.com/locate/jorganchem

Theoretical study on copper-catalyzed reaction of hydrosilane, alkyne and carbon dioxide: A hydrocarboxylation or a hydrosilylation process ?

Yi Zhao [a,c], Yuxia Liu [b], Siwei Bi [b,*], Yongjun Liu [a,*]

[a] Northwest Institute of Plateau Biology, Chinese Academy of Sciences, Xining, Qinghai 810001, China
[b] School of Chemistry and Chemical Engineering, Qufu Normal University, Qufu 273165, PR China
[c] School of Chemical Engineering, Shandong University of Technology, Zibo 255049, PR China

ARTICLE INFO

Article history:
Received 18 June 2013
Received in revised form
22 July 2013
Accepted 25 July 2013

Keywords:
Hydrocarboxylation
Hydrosilylation
σ bond metathesis
Insertion
Carbon dioxide
DFT

ABSTRACT

The hydrocarboxylation and hydrosilylation processes proposed in the copper-catalyzed reaction among carbon dioxide, diphenylacetylene and $HSi(OEt)_3$ were comparatively studied with the aid of density functional theory calculations. Our study is to explore why the reaction preferred a hydrocarboxylation rather than a hydrosilylation process. It was found that the σ bond metathesis between Cu–C and H–Si involved in the hydrosilylation process had a significantly high reaction barrier in the presence of CO_2 (47.4 kcal/mol). Instead, CO_2 insertion and the subsequent σ bond metathesis between Cu–O and H–Si involved in the hydrocarboxylation process were confirmed kinetically feasible, consistent with the experimental facts.

1. Introduction

CO_2 is inexpensive, easy-to-handle, and nontoxic, so it can be considered as an ideal, renewable carbon unit in organic synthesis [1–4]. However, thermodynamic considerations limit the widespread application of CO_2 in chemical reactions owing to its chemical inertness. Recently, researchers found that CO_2 could be activated by many transition metal complexes [5–10]. For example, transition metal-catalyzed carboxylation of organozinc and organoboron compounds can transform CO_2 into useful organic compounds [11–14]. In addition, hydrocarboxylation [15–17] of C–C multiple bonds with CO_2, such as the nickel-bipyridine-catalyzed electroreductive coupling of 1,3-diynes and 1,3-enynes with CO_2, is also very promising. However, the indispensable reducing agents, such as $ZnEt_2$ and $AlEt_3$, are extremely air sensitive. To solve this question, Tsuji and his coworkers reported the copper-catalyzed hydrocarboxylation of alkynes with CO_2 (balloon) and hydrosilane as reducing agents, leading to the products of α,β-unsaturated carboxylic acids [18]. In this experiment, the [IMesCuF] was proved to be the effective catalyst compared with [IPrCuCl] + *t*BuONa, [IMesCuCl] + *t*BuONa, and [IPrCuF]. With [IMesCuF] as the catalyst, $HSi(OEt)_3$ was found to be the best reducing agent compared with PMHS, $HSi(O^iPr)_3$, and H_2SiPh_2. As shown in Scheme 1, the hydrocarboxylation reaction was experimentally confirmed feasible, giving the carboxyl silane product **P** with high regioselectivity. But the direct hydrosilylation reaction between **R1** and **R2**, leading to the formation of alkenyl silane product **P′**, was found not available.

Possible catalytic cycle has been proposed for the stoichiometric reaction (Scheme 2). IMesCuH, generated from IMesCuF, was proposed to be the real catalyst. For the hydrocarboxylation process, three steps are involved: step I is an insertion of C–C triple bond into Cu–H, generating an alkenyl copper complex (**4**); step II involves CO_2 insertion into Cu–C, leading to the formation of a carboxyl compound (**6**); step III is related to a σ-bond metathesis between Cu–O and H–Si, giving product **P**. The unavailable hydrosilylation process is proposed to undergo a direct σ-bond metathesis between Cu–C and H–Si, giving product **P′**. Recently, Wu and co-workers reported a similar theoretical study on the hydrocarboxylation process [19]. They studied the mechanism for the Cu(I)-mediated domino reaction of asymmetrical alkynes with CO_2 by the reducing reagent of hydrosilane, giving a product in good yield with high regioselectivity. They give the factors, steric and electronic

* Corresponding authors.
E-mail addresses: siweibi@126.com (S. Bi), yongjunliu_1@sdu.edu.cn (Y. Liu).

0022-328X/$ – see front matter © 2013 Elsevier B.V. All rights reserved.
http://dx.doi.org/10.1016/j.jorganchem.2013.07.065

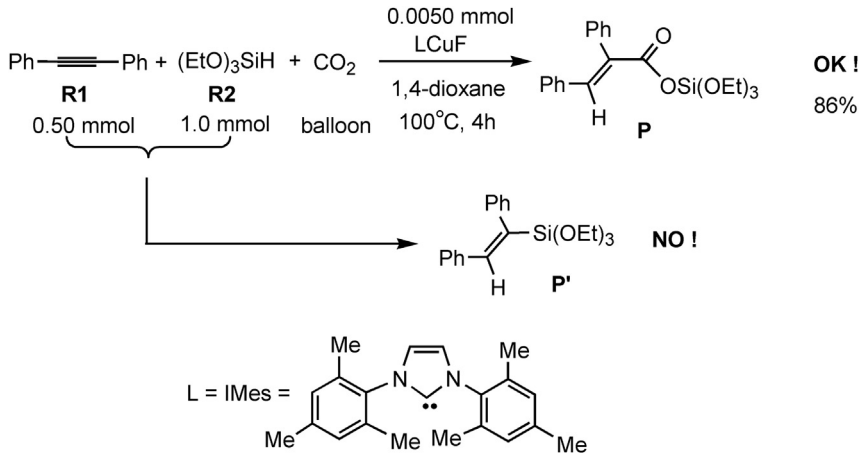

Scheme 1. Hydrocarboxylation of diphenylacetylene (**R1**) using a hydrosilane (**R2**) and CO_2.

effects, which determine the regioselectivity. In this work, we aim to make clear why the copper-catalyzed reaction prefers a hydrocarboxylation process rather than a hydrosilylation one.

Although the catalytic cycle for the reaction studied here has been proposed, the reason for the reaction undergoing hydrocarboxylation rather than hydrosilylation is still remained unclear. This question is also raised by Zhang et al. in a highlight article [20] and Lin et al. in a feature article [21]. As is known, the mechanistic details of a reaction are not easily accessible by experiments. Theoretical and computational study has remarkable advantages in this regard. The geometric structures of reactants, intermediates, transition states and products can be located, and related thermodynamic and kinetic data can be obtained with the help of quantum chemistry calculations. Thus, theoretical and computational study could offer the access to mechanistic details of a reaction, and provide further understanding for experimental observations and would possibly provide helpful information for designing new related reactions. In this paper, we present a density functional theory (DFT) study on the copper-catalyzed hydrocarboxylation of alkynes with CO_2 reported by Tsuji et al., with the aim to make clear why the reaction undergoes a hydrocarboxylation process instead of a hydrosilylation process.

2. Computational details

In our calculations, all molecular geometries were optimized at the B3LYP level of DFT [22–25]. To identify all stationary points as minima (zero imaginary frequencies) or transition states (one imaginary frequency), we calculated frequencies at the same level of theory. All the transition states were checked by intrinsic reaction coordinate (IRC) [26,27] analysis. To describe C, O, N, F, Si and H atoms, we used standard 6–31G(d,p) basis sets. To describe Cu atom, we used the 6–311G(d) Wachters–Hay basis set [28–30]. The solvent effect was examined by performing single-point self-consistent reaction field (SCRF) calculations based on the polarizable continuum model (PCM) [31–33] for all the gas-phase optimized species. The atomic radii used for the PCM calculations were specified using the UAKS keyword. In Gaussian 03, the PCM parameters are not available for 1,4-dioxane. We instead used the parameters of benzene for PCM calculations because the dielectric constant of 1,4-dioxane ($\varepsilon = 2.2099$) is very close to that of benzene ($\varepsilon = 2.2706$). All calculations were performed with the Gaussian 03 software package [34]. To probe the detailed reaction mechanisms and present further understanding of such kind of reactions, we use IMesCuF and $HSi(OEt)_3$ as the reagents, which can generate the active catalyst IMesCuH. In all of the figures of potential energy profiles, the calculated solvation-corrected relative free energies (kcal/mol) and relative enthalpic energies (kcal/mol, in parentheses) were presented. Because of the entropic contribution, the relative free energies and relative enthalpic energies are significantly different in cases where the numbers of reactant and product molecules are not equal. In this paper, relative free energies are used to analyze the reaction mechanisms.

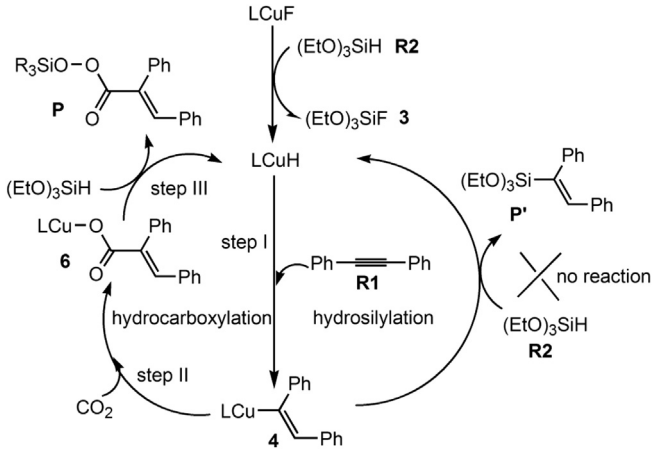

Scheme 2. Plausible catalytic cycle.

3. Results and discussion

3.1. Generation of the active catalyst IMesCuH

The calculated potential free energy profile for generation of the active catalyst IMesCuH is shown in Fig. 1, where relative energy of the resulting IMesCuH is set to be zero reference point. As illustrated in Fig. 1, generation of the active catalyst IMesCuH is a direct silicon-to-copper transmetalation between IMesCuF and $HSi(OEt)_3$ (**R2**). Key geometric structures together with selected bond distances are shown in Fig. 2.

IMesCuF and **R2** firstly form a four-membered intermediate (**1**). It is found that even from intermediate **1** Cu–F and Si–H bonds can be effectively activated by Si and Cu centers, respectively. The Cu–F bond length increases from 1.754 Å to 1.894 Å and the Si–H elongates from 1.463 Å to 1.539 Å. Step **1** to **2** via $\mathbf{TS_{1-2}}$ is actually a σ bond metathesis leading to the formation of Cu–H and Si–F σ bonds. As shown in the geometry of intermediate **2**, Cu–H and Si–F are calculated to be 1.621 Å and 1.725 Å, respectively. The activation barrier for the step

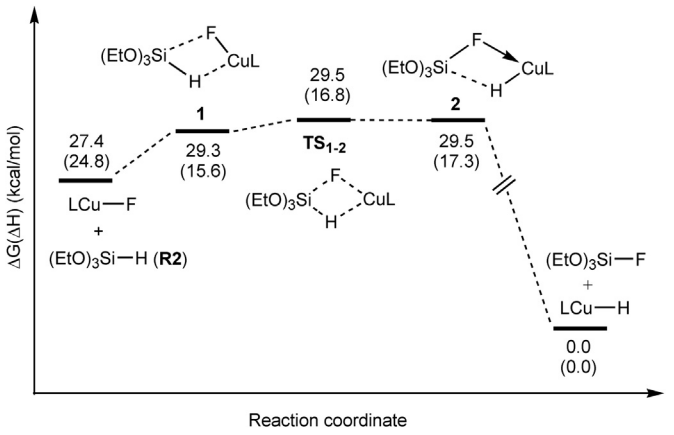

Fig. 1. Potential free energy profile for generation of the active catalyst LCuH (L = IMes). The relative free energies and relative enthalpic energies (in parentheses) are given in kcal/mol.

(**1** → **2**) is calculated to be only 0.2 kcal/mol, indicating that σ bond metathesis can occur very readily. Subsequently, removal of $(EtO)_3SiF$ from **2** generates the catalyst IMesCuH with a big energy decrease (−29.5 kcal/mol). The small overall barrier (2.1 kcal/mol, LCuF + **R2** to $\mathbf{TS_{1-2}}$) and large free energy decrease (−27.4 kcal/mol) indicate the active catalyst IMesCuH can be obtained very easily, which is in accordance with the experimental observations that the active catalyst could be obtained quickly at room temperature [35].

3.2. Insertion of the alkyne (*R1*) into Cu–H bond of IMesCuH

The potential energy profile for insertion of **R1** into Cu–H bond of IMesCuH to afford intermediate **4** is shown in Fig. 3. Key geometric structures together with the selected bond distances are illustrated in Fig. 4.

Firstly, **R1** coordinates to the Cu center to form adduct **3**. The C–C triple bond increases from 1.208 Å in **R1** to 1.277 Å in **3**, indicating this bond has been efficiently activated. Then, an

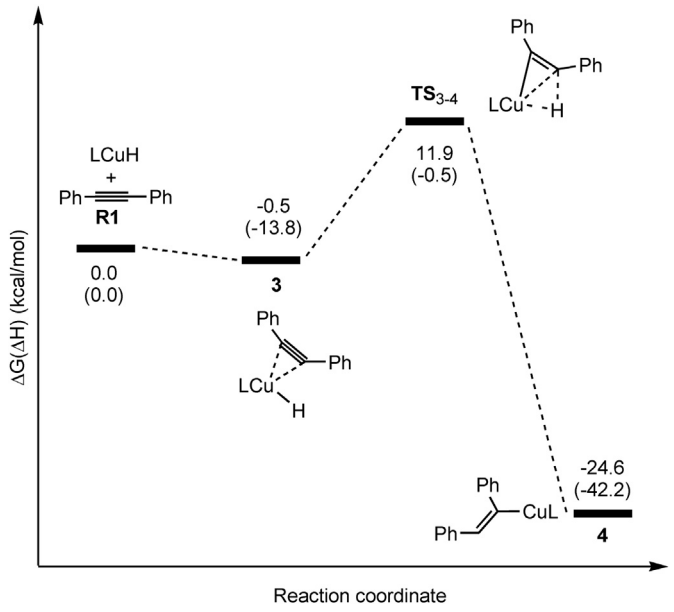

Fig. 3. Potential energy profile for insertion of the alkyne (**R1**) into Cu–H bond of LCuH (L = IMes). The relative free energies and relative enthalpic energies (in parentheses) are given in kcal/mol.

alkyne insertion into Cu–H bond occurs, leading to the insertion product **4**. The insertion barrier from **3** to $\mathbf{TS_{3-4}}$ is calculated to be 12.4 kcal/mol and the reaction free energy change (**R1** + LCuH to **4**) is calculated to be −24.6 kcal/mol, suggesting that the insertion product can be easily available under the reaction conditions.

3.3. Comparison between the hydrocarboxylation and the hydrosilation processes

Experiments have confirmed that the hydrocarboxylation occurred while the hydrosilylation could not under the reaction conditions (Scheme 1). For probing the reason, we explored the

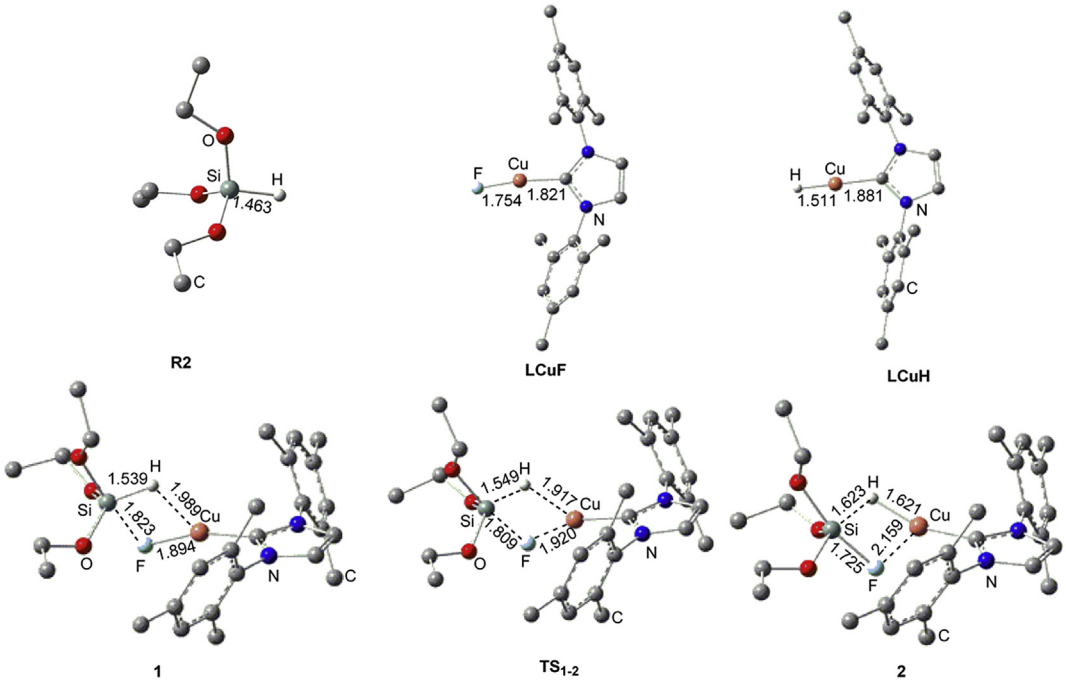

Fig. 2. Calculated geometric structures together with key structural parameters (Å) for the species shown in Fig. 1. For clarity, the hydrogen atoms attached to carbon atoms are omitted.

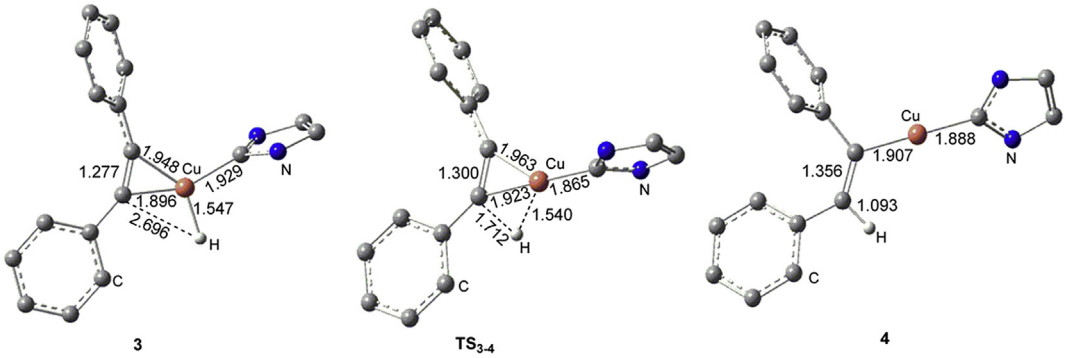

Fig. 4. Calculated geometric structures together with key structural parameters (Å) for selected species shown in Fig. 3. For clarity, some hydrogen atoms attached to carbon atoms or groups attached to the N atoms are omitted.

possible reaction mechanisms for both the hydrocarboxylation and the hydrosilylation processes (Scheme 2). The potential energy profile involving the hydrocarboxylation process (path a) and the one involving the hydrosilylation process (path b) were shown in Fig. 5. Geometric structures together with selected structural parameters for key species were illustrated in Fig. 6.

3.3.1. *Path a: hydrocarboxylation process*

Path a presents the detailed reaction mechanism of hydrocarboxylation process. Intermediate **4** firstly forms a complex adduct **5** with CO_2 through van der Vaals interactions because CO_2 is relatively far away from the alkenyl copper complex in **5**. As shown in Fig. 6, Cu–C3 and Cu–O2 in **5** were calculated to be 3.238 Å and 3.713 Å, respectively. Step **5** → **6** is the insertion of CO_2 into the Cu–C bond with the oxygen toward the Cu center, affording a carboxyl copper complex (**6**). In $\mathbf{TS_{5-6}}$, CO_2 is found to be non-coplanar with the Cu–C moiety, similar to the transition state of CO_2 insertion into Cu–Ph calculated by Lin's group [36]. The interaction between CO_2 and the LCu–alkenyl complex is believed to be a nucleophilic attack of the Cu–C σ bond on the CO_2 carbon [36]. Intermediate **6** isomerizes into the more stable intermediate **7** through the O1–C3 σ bond rotation. The instability of **6** compared to **7** can be attributed to non-planarity of the O=C–C=C moiety that is caused by the steric hindrance between the terminal phenyl group and the group attached to the N atom. Dihedral angles of the O=C–C=C moiety in **6** and **7** were calculated to be 139.0° and 168.3°, respectively. Clearly, more effective conjugation of the O=C–C=C moiety is present in **7**, leading to the intermediate being more stable. In summary, the overall free energy barrier for the CO_2 insertion process is computed to be 14.2 kcal/mol (**4** to $\mathbf{TS_{5-6}}$), and the free energy change for the process is −14.6 kcal/mol (**4**–**7**). Therefore, the CO_2 insertion process could occur easily under the reaction conditions. By the way, the insertion of CO_2 with the carbon atom toward the Cu center has been found not available [36]. Our calculations show that the free energy barrier for such an insertion process is as high as 61.1 kcal/mol.

The subsequent two steps (**7** → **8** → **P**) are related to a σ bond metathesis process between Cu–O and Si–H. Intermediate **7** and $(EtO)_3SiH$ first form an intermediate **8** through van der Waals interactions where the closest distance between the two species is the Cu···HSi distance (2.690 Å). The last step **8** to **P** is a typical σ bond metathesis where both the Cu–O and Si–H bonds are broken

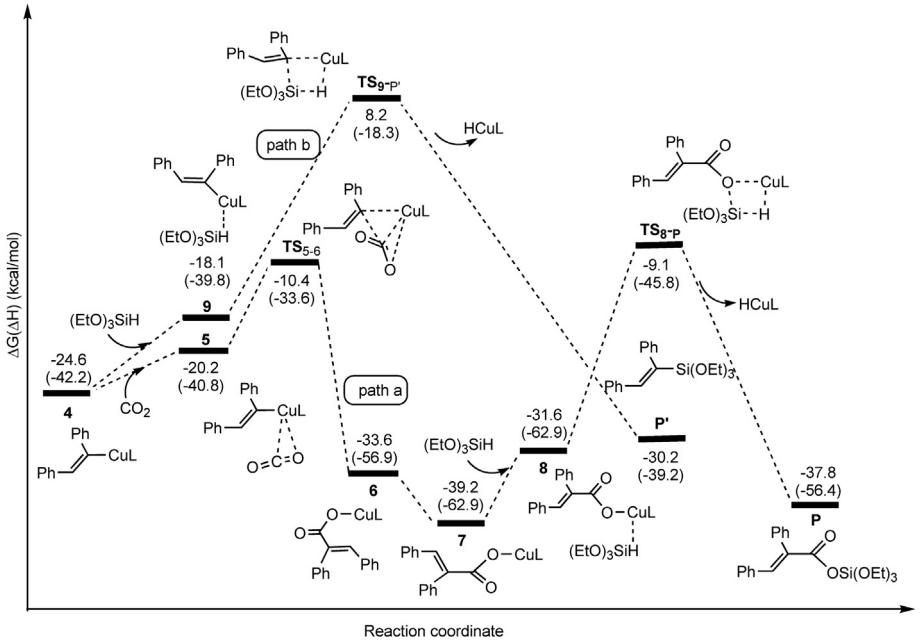

Fig. 5. Potential energy profiles leading to the hydrocarboxylated product (**P**) (path a) and the hydrosilated product (**P′**) (path b). The relative free energies and relative enthalpic energies (in parentheses) are given in kcal/mol.

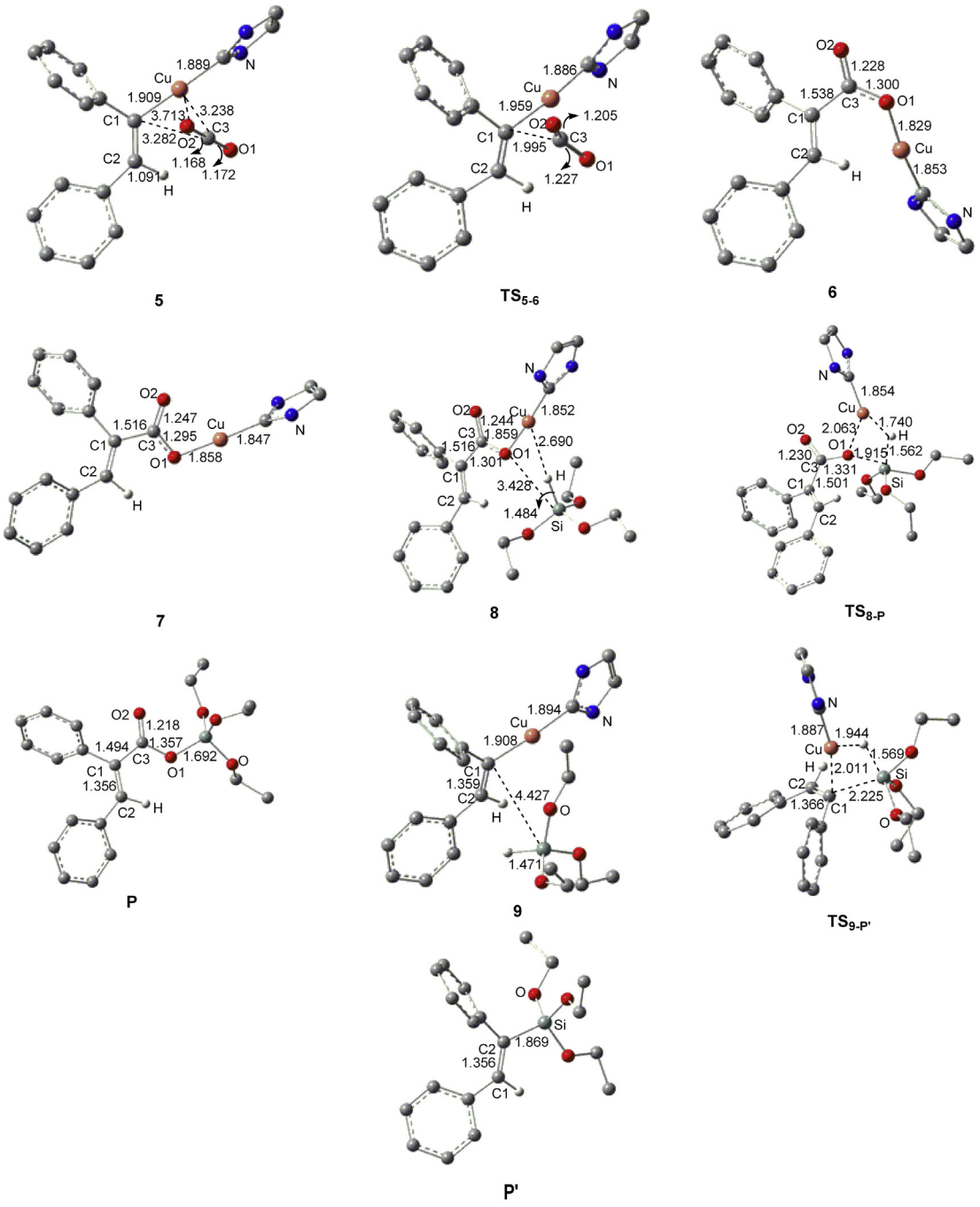

Fig. 6. Calculated geometric structures together with key structural parameters (Å) for the species shown in Fig. 5. For clarity, some hydrogen atoms attached on carbon atoms or the groups attached on the N atoms are omitted.

and correspondingly the Cu–H and Si–O bonds are formed. The overall free energy barrier for the metathesis process is computed to be 30.1 kcal/mol (**7** to $\mathbf{TS_{8-P}}$). Such a barrier height is reasonable for the reaction temperature of 100 °C. It can be seen from the whole reaction mechanism (**R1** to **P**) presented in Figs. 5 and 6 that the rate-determining process is predicted to be the σ bond metathesis process (**7** to **P**).

3.3.2. Path b: hydrosilylation process

The hydrosilylation process, which is also regarded as a transmetalation process, was proposed as shown in Fig. 6 (path b). Intermediate **4** and the hydrosilane first form the intermediate **9** through van der Waals interaction. Then, **9** via the transition state $\mathbf{TS_{9-P'}}$ undergoes a σ bond metathesis process between Cu–C and Si–H, generating **P′** and regenerating the catalyst IMesCuH. Since intermediate **4** first transforms into the more stable **7** in the presence of CO_2, the overall rate-determining process for the hydrosilylation process is hence considered to be **7** → **4** → **P′**. Thus, the overall free activation energy would be 47.4 kcal/mol (**7** to $\mathbf{TS_{9-P'}}$), noticeably higher than that of hydrocarboxylation process (30.1 kcal/mol, **7** to $\mathbf{TS_{8-P}}$). Therefore, the calculation results confirm that the reaction studied in this work undergoes a hydrocarboxylation process but not a hydrosilylation process. We also note that the barrier for the hydrosilylation process would be 32.8 kcal/mol in the absence of CO_2.

3.3.3. Discussion on the hydrosilylation and hydrosilylation processes

Our calculation results support the experimental observations that the reaction prefers a hydrocarboxylation process over a hydrosilylation process. To gain a better understanding of the chemoselectivity, it is necessary and valuable to get insight into the origin why the hydrocarboxylation process is preferred.

(1) High hydrosilylation barrier leads to the reaction preferring CO_2 insertion.

Clearly, the reaction undergoing CO_2 insertion rather than hydrosilylation is caused by the high hydrosilylation barrier (**4** → **TS$_{9-P'}$**). By carefully examining the geometry of **TS$_{9-P'}$**, we found that the strongly forced steric hindrance is involved in the transition state. To understand the steric influence on the relative stability of **TS$_{9-P'}$** we carried out a simple energy decomposition analysis (EDA) [37–39] (Fig. 7). Relative enthalpic energies (kcal/mol) in gas phase are used to describe the EDA process. The barrier in enthalpic energy for the hydrosilylation process was calculated to be 26.7 kcal/mol, similar to that in solution (23.9 kcal/mol). Geometries of fragments **F$_4$** and **F$_{R2}$** were directly derived from **TS$_{9-P'}$** and their relative enthalpic energies were obtained by single point energy calculations. ΔH1 represents distortion energy of the alkenyl copper complex (**4** to **F$_4$**) and ΔH2 represents distortion energy of the hydrosilane (**R2** to **F$_{R2}$**). ΔH3 denotes the attraction energy between **F$_4$** and **F$_{R2}$**. Clearly, ΔH = ΔH1 + ΔH2 + ΔH3. ΔH1 and ΔH2 are responsible for the energy rise from **4** + **R2** to **TS$_{9-P'}$**, with the latter distortion energy predominating (33.5 kcal/mol). In other words, significant geometric distortion from **R2** to **F$_{R2}$** is an important factor leading to the transition state high in energy. Strong steric hindrance of the alkenyl group with the incoming hydrosilane causes significant geometric distortion of the hydrosilane. As the same geometry distortion could happen in the hydrocarboxylation (**TS$_{8-P}$**), we also carried out a similar energy decomposition analysis (EDA) (Fig. 8). The barrier in enthalpic energy for the hydrocarboxylation process calculated in gas phase is 16.8 kcal/mol, similar to that in solution (17.1 kcal/mol). The energy increases caused by distortion of the carboxyl cooper complex (**7** to **F$_7$**) and the hydrosilane (**R2** to **F′$_{R2}$**) are similar (22.1 vs. 22.4 kcal/mol). The hydrosilane in **TS$_{8-P}$** is found to be less seriously distorted than in **TS$_{9-P'}$** (22.4 vs. 33.5 kcal/mol). This is understandable because the presence of COO moiety in **TS$_{8-P}$** leads to smaller steric hindrance between the hydrosilane and the alkenyl group compared to the hindrance in **TS$_{9-P'}$**. Clearly, the alkenyl copper complex (**4**) prefers to undergo CO_2 insertion (**4** → **TS$_{5-6}$**, $\Delta G^{\neq}$ = 14.2 kcal/mol) over the hydrosilylation (**4** → **TS$_{9-P'}$**, $\Delta G^{\neq}$ = 32.8 kcal/mol).

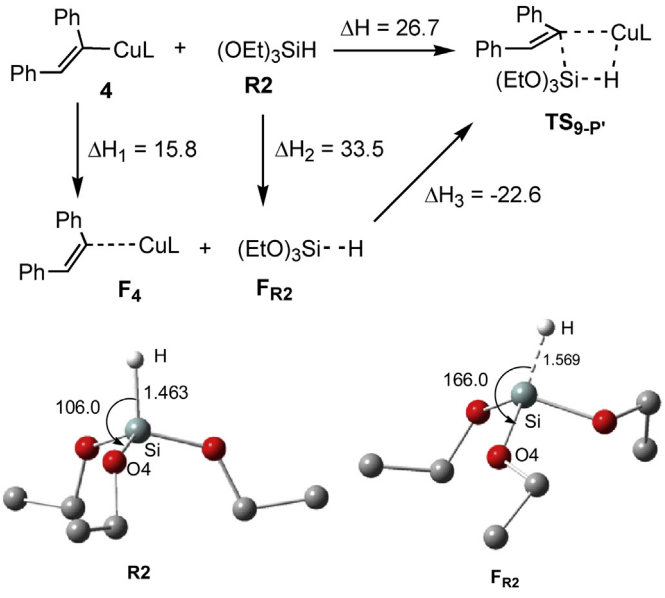

Fig. 7. Energy decomposition analysis (EDA) from **4** + **R2** to **TS$_{9-P'}$**. The relative enthalpic energies are given in kcal/mol. Geometries of **R2** and **F$_{R2}$** together with key parameters are also presented. For clarity, the H atoms attached to C atoms are omitted. The bond distances are given in Å and the bond angles are given in degree.

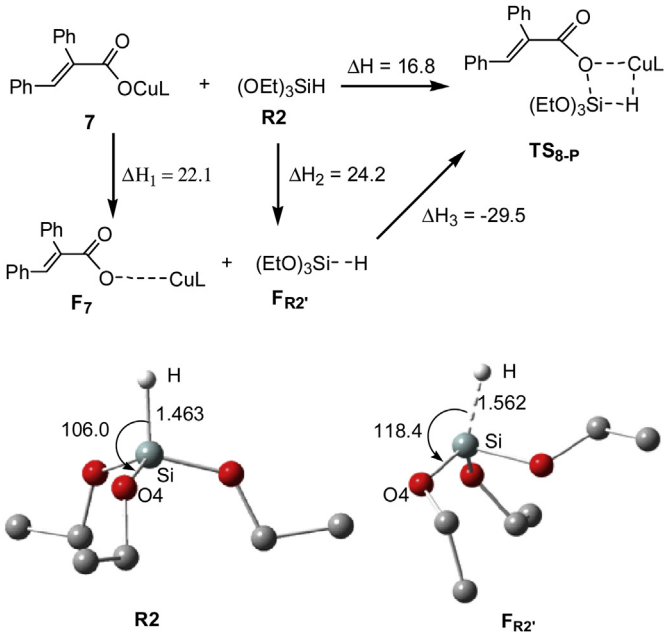

Fig. 8. Energy decomposition analysis (EDA) from **7** + **R2** to **TS$_{8-P}$**. The relative enthalpic energies are given in kcal/mol. Geometries of **R2** and **F′$_{R2}$** together with key parameters are also presented. For clarity, the H atoms attached to C atoms are omitted. The bond distances are given in Å and the bond angles are given in degree.

(2) Role of the carboxyl copper complex (**7**) in supporting the hydrocarboxylation process.

As can be seen from Fig. 5, the insertion product **7** is a resting state for both hydrocarboxylation and hydrosilylation. The activation process for hydrocarboxylation is from **7** to **TS$_{8-P}$** with a barrier of 30.1 kcal/mol, while that for hydrosilylation is from **7** via **4** to **TS$_{9-P'}$** with a barrier of 47.4 kcal/mol. Clearly, formation of insertion product **7** increases the hydrosilylation barrier, making the process prohibitively accessible. Therefore, both kinetically and thermodynamically favorable CO_2 insertion leads to the reaction undergoing hydrocarboxylation instead of hydrosilylation.

4. Conclusions

The copper-catalyzed reaction among diphenylacetylene, CO_2 and $HSi(OEt)_3$ has been theoretically investigated by means of density functional theoretical calculations, with the aim to make clear why the reaction prefers a hydrocarboxylation process rather than a hydrosilylation one. Our findings are as follows:

(1) The catalytically active species IMesCuH can be very readily obtained.
(2) Insertion of diphenylacetylene into Cu–H of IMesCuH can be easily accessible.
(3) For the hydrocarboxylation process, CO_2 insertion into Cu–C bond of the copper alkenyl complex and the subsequent σ bond metathesis between Cu–O and H–Si were proved kinetically

feasible under the reaction conditions. The metathesis process was found to be rate-determining with a barrier of 30.1 kcal/mol.

(4) For the hydrosilylation process, the σ bond metathesis between Cu–C and H–Si was found to be kinetically unavailable with a barrier of 47.4 kcal/mol in the presence of CO_2. Strongly forced geometric distortion of $(EtO)_3SiH$ in the metathesis transition state was found to be an important factor in raising the metathesis barrier.

(5) Formation of the more stable CO_2 insertion product (**7**) plays an important role in blocking the reaction to undergo a hydrosilylation process.

(6) This study would provide helpful information in designing related hydrocarboxylation or hydrosilylation reactions.

Acknowledgments

This work was supported by the National Natural Science Foundation of China (Grant Nos. 21173126 and 21173129) and Sci-Tech Research Project of Shandong Colleges and Universities (J10LB10).

References

[1] T. Sakakura, J. Choi, H. Yasuda, Chem. Rev. 107 (2007) 2365–2387.
[2] D.J. Darensbourg, Chem. Rev. 107 (2007) 2388–2410.
[3] A. Correa, R. Martin, Angew. Chem. Int. Ed. 48 (2009) 6201–6204.
[4] I.I.F. Boogaerts, S.P. Nolan, Chem. Commun. 47 (2011) 3021–3024.
[5] T. Beweries, V.V. Burlakov, S. Peitz, P. Arndt, W. Baumann, A. Spannenberg, U. Rosenthal, Organometallics 27 (2008) 3954–3959.
[6] J. Takaya, S. Tadam, K. Ukai, N. Iwasawa, Org. Lett. 10 (2008) 2697–2700.
[7] T. Ohishi, M. Nishimura, Z. Hou, Angew. Chem. Int. Ed. 47 (2008) 5792–5795.
[8] A. Correa, R. Martin, J. Am. Chem. Soc. 131 (2009) 15974–15975.
[9] Y. Tsuj, T. Fujihara, Chem. Commun. 48 (2012) 9956–9964.
[10] T. Fujihara, Y. Tani, K. Semba, J. Terao, Y. Tsuji, Angew. Chem. Int. Ed. 51 (2012) 11487–11490.
[11] C.S. Yeung, V.M. Dong, J. Am. Chem. Soc. 130 (2008) 7826–7827.
[12] M.J.H. Ochiai, K. Hirano, H. Yorimitsu, K. Oshima, Org. Lett. 10 (2008) 2681–2683.
[13] T. Ohishi, M. Nishiura, Z. Hou, Angew. Chem. Int. Ed. 120 (2008) 5876–5877.
[14] K. Ukai, M. Aoki, J. Takaya, N. Iwasawa, J. Am. Chem. Soc. 128 (2006) 8706–8707.
[15] S. Drien, E. Duach, J. Prichon, J. Am. Chem. Soc. 113 (1991) 8447–8454.
[16] C.M. Williams, B. Jeffrey, J.B. Johnson, T. Rovis, J. Am. Chem. Soc. 130 (2008) 14936–14937.
[17] J. Takaya, N. Iwasawa, J. Am. Chem. Soc. 130 (2008) 15254–15255.
[18] T. Fujihara, T. Xu, K. Semba, J. Terao, Y. Tsuji, Angew. Chem. Int. Ed. 50 (2011) 523–527.
[19] Q. Wang, et al., J. Organomet. Chem. (2013), http://dx.doi.org/10.1016/j.jorganchem.2012.1012.029.
[20] Y. Zhang, S.N. Riduan, Angew. Chem. Int. Ed. 50 (2011) 6210–6212.
[21] T. Fan, X. Chen, Z. Lin, Chem. Commun. 48 (2012) 10808–10828.
[22] A.D. Becke, J. Chem. Phys. (1993) 5648–5652.
[23] B. Miehlich, A. Savin, H. Stoll, H. Preuss, Chem. Phys. Lett. (1989) 200–206.
[24] C. Lee, W. Yang, G. Parr, Phys. Rev. B 37 (1988) 785–788.
[25] P.J. Stephens, F.J. Devlin, C.F. Chabalowski, J. Phys. Chem. 98 (1994) 11623–11627.
[26] K. Fukui, J. Phys. Chem. 74 (1970) 4161–4163.
[27] k. Fukui, Acc. Chem. Res. 14 (1981) 363–368.
[28] A.J.H. Wachters, J. Chem. Phys. 52 (1970) 1033–1036.
[29] P.J. Hay, J. Chem. Phys. 66 (1977) 1306–1316.
[30] M. Wang, Z. Lin, Organometallics 29 (2010) 3077–3084.
[31] V. Barone, M. Cossi, J. Phys. Chem. A 102 (1998) 1995–2001.
[32] M. Cossi, N. Rega, G. Scalmani, V. Barone, J. Comput. Chem. 24 (2003) 669–681.
[33] J. Tomas, B. Mennucc, R. Cammi, Chem. Rev. 105 (2005) 2999–3094.
[34] M.J.E.A. Frisch, Gaussian 03, Revision C.02, Gaussian, Inc., Pittsburgh, PA, 2004.
[35] J.R. Herron, Z.T. Ball, J. Am. Chem. Soc. 130 (2008) 16486–16487.
[36] L. Dang, Z. Lin, T.B. Marder, Organometallics 29 (2010) 917–927.
[37] F.M. Bickelhaupt, J. Comput. Chem. 20 (1999) 114–128.
[38] A. Ariafard, Z. Lin, J. Am. Chem. Soc. 128 (2006) 13010–13016.
[39] A. Ariafard, Z. Lin, Organometallics 25 (2006) 5788–5794.